

# Impedance Matching Network of Passive Coupler with Coaxial Cable for Airborne Sonar Applications

G. Manoj,<sup>1,2\*</sup> R. Ramesh<sup>1</sup> and S. O. Kundukulam<sup>1</sup>

<sup>1</sup> Naval Physical and Oceanographic Laboratory, DRDO, Thrikkakara, Kochi, India

<sup>2</sup> Cochin University of Science and Technology, Kochi, India

The manuscript was received on 30 July 2022 and was accepted after revision for publication as research paper on 22 February 2023.

## Abstract:

*A design methodology is proposed to implement an impedance-matching network in a high-power underwater acoustic transmitting system to minimize power loss through long cables. For this, a Lumped-parameter electrical equivalent circuit model has been developed to analyze the transmitting system along with various couplers and decouplers introduced for simultaneous transmission of data and DC power along with high-power AC. The effects of these couplers on the end performance of the system have been studied and compensated for by suitably modifying the impedance matching lines (ML). The appropriate impedance matching lines significantly enhance the power by about 300 watts and improve the power factor to 100 %.*

## Keywords:

*airborne sonar, coupling, equivalent circuit, impedance matching, tuning coil, underwater transducer*

## 1 Introduction

Power transfer from an onboard power amplifier unit to a projector located at a remote unit through a long, single-core coaxial cable is one of the fundamental issues in designing airborne sonar systems. Power loss occurs mainly due to attenuation in the cable, which increases with an increase in the frequency and length of the cable [1, 2]. In addition, the electrical impedance mismatch between the cable and the transducer and the one between the power amplifier and the cable results in the reflection of electrical energy back into the power amplifier, causing undesirable degradation in system performance [3]. The power loss is to be adequately compensated to obtain optimum system performance.

---

\* Corresponding author: Naval Physical and Oceanographic Laboratory, Defence Research and Development Organisation, Thrikkakara, Kakkanad, Ernakulam, India. Phone: +91 94 97 81 29 61, E-mail: manojg.npol@gov.in. ORCID 0000-0002-0310-4935.

In the present case, the cable has two interfaces, one with the power amplifier at the onboard end and the other with the transducer at the remote end. Impedance matching at these interfaces has been accomplished in the present work by implementing a lumped parameter equivalent circuit model. For airborne sonar applications, in addition to acoustic signal transmission, high-speed data and high-voltage DC are simultaneously transmitted through the same cable. The above scenario can be implemented using a relay-based or passive filter-based coupling scheme [4]. In the relay-based coupling scheme, frequent switching of cable is required for power transmission and DC and data. When the cable is switched for high-power transmission, there should be no DC supply at the remote side. For proper transmission of high-speed data, continuous power should be available on the remote side. Hence for relay-based coupling, a power backup is required at the remote side. In this paper, a passive coupling scheme has been designed and discussed to overcome the relay based coupling scheme power backup need. In this scheme, there can be a considerable power loss due to impedance mismatch because of the addition of couplers into a long cable. Here we introduce a novel approach for reducing the power loss due to long cable, AC coupler, DC coupler, and Data coupler by adding a tuning coil and a matching line (ML).

The above scheme helps to replace the use of a multicore cable with a single-core coaxial cable. Here it is essential to isolate the high-power AC signals from the high-voltage DC and data flowing through the same line. The block diagram describing the high-power signal transmission system through AC coupler, DC coupler Data Coupler and corresponding de-couplers, single-core coaxial cable, onboard unit, and the remote unit is shown in Fig. 1.

Including reactive components, such as capacitors and inductors of the coupler and de-coupler circuits, introduces additional impedance mismatch. The AC signal is coupled to the single-core coaxial cable through an AC coupler and decoupled at the cable's other end before feeding to the transducer. Similarly, the DC and Data are coupled at the onboard end of the cable through the DC coupler and the Data coupler, respectively, and they are decoupled at the remote end of the cable using DC and Data de-couplers.

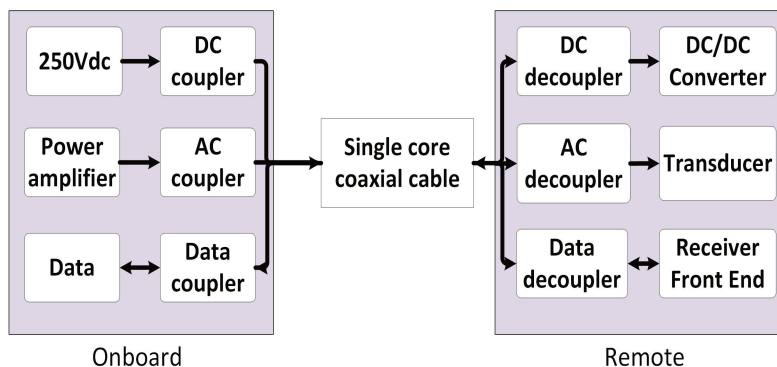


*Fig. 1 Block diagram of the underwater acoustic transmitting system*

The present work describes the design, equivalent circuit modeling, MultiSim simulation, and experimental validation of an impedance matching scheme to deliver maximum power from the power source onboard to the remote underwater transducer through a long, single-core coaxial cable. The theoretical analysis results have been

verified by Multisim circuit simulation studies and validated by experimental studies. The impedance matching technique, theoretical analysis (equivalent circuit analysis based on circuit theory), simulation results (refer to Multisim simulation tool analysis), and experimental results are presented in this paper.

## 2 Electrical Equivalent Circuit Model

### 2.1 Underwater Transducer

An underwater transmitting transducer or projector operating at a frequency close to its resonance can be represented as a lumped-parameter electrical equivalent circuit [5, 6], as shown in Fig. 2. The components  $R_1$ ,  $L_1$  and  $C_1$  are the electrical equivalents of the modal loss, mass, and compliance, and  $C_0$  is the dielectric capacitance of the piezoelectric transducer [1, 7-9]. The input electrical impedance of the transducer  $Z_T$  is written in terms of circuit parameters as given by the relation,

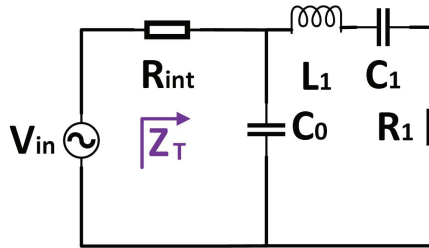


Fig. 2 Equivalent circuit of a piezoelectric transducer at resonance

$$\frac{1}{Z_T} = Y_T = j\omega C_0 + \frac{\omega C_1 (j - j\omega^2 C_1 L_1 + \omega C_1 R_1)}{1 + \omega^2 C_1 [L_1 (\omega^2 C_1 L_1 - 2) + C_1 R_1^2]} \quad (1)$$

The in-water input electrical admittance of the transducer is measured with small signals, but the results may slightly differ for a high-power signal. However, all the transducer measurements are taken in linear regions with high-power signals, where the total harmonic distortion (THD) is less than a few percent. Therefore, small signal measurements are not expected to cause a significant error. Hence measurement values of admittance with small signals are subsequently used to determine the equivalent circuit parameters [9-11], namely  $R_1$ ,  $L_1$ ,  $C_0$  and  $C_1$ . These parameters are refined by least-squares fitting to Eq. (1) using the procedure described elsewhere [12].

This method has been verified by plotting the theoretical conductance  $G$ , admittance  $B$  and the measured data, as shown in Fig. 3. The close agreement validates the model and the method used in this analysis. Therefore, the transducer can be fully represented by the equivalent circuit shown in Fig. 2. Tab. 1 shows the parameters of the transducer equivalent circuit.

### 2.2 Tuning Coil

As seen in Fig. 2, the input impedance of the transducer is reactive and has a significant contribution from the imaginary part. This results in loss of power and reduction in Power Factor ( $PF$ ) given by,

$$PF = \cos \phi = \frac{G}{|Y|} \quad (2)$$

where  $\phi$  is the phase angle in radians. The capacitive reactance of a piezo ceramic transducer can be tuned out by connecting a shunt inductor  $L_{TC}$  [1], whose value is determined from

$$L_{TC} = \frac{1}{C_0 \omega^2} \quad (3)$$

Tab. 1 Equivalent circuit parameter of the transducer

Parameters	Values
$C_0$ [nF]	54.6
$R_1$ [k $\Omega$ ]	1.552
$L_1$ [H]	0.385
$C_1$ [nF]	2.9

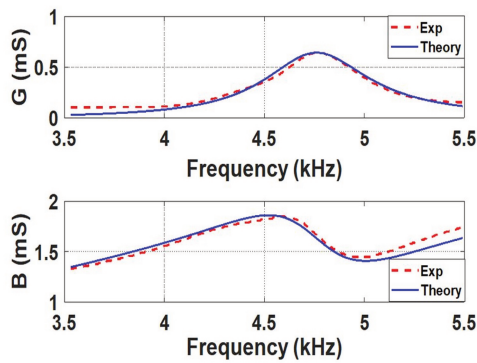


Fig. 3 Theoretical and measured spectra of conductance ( $G$ ) and susceptance ( $B$ ) of the bare transducer

The tuned transducer presents a purely resistive load to the driving power amplifier so that  $Z_T = R_T$  at resonance. The equivalent circuit of the transducer connected with a tuning coil  $L_{TC}$  [13] is shown in Fig. 4. The power amplifier is represented by a voltage source  $V_{in}$  in series with internal resistance  $R_{int}$ . The input impedance of the tuned transducer  $Z_{TT}$ , as seen by the power amplifier, is

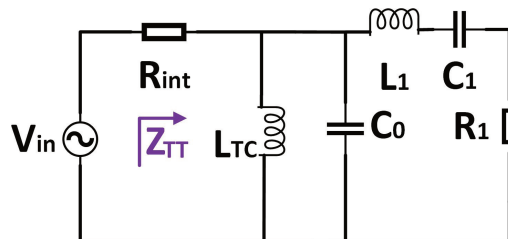


Fig. 4 Equivalent circuit of the transducer with inductive shunt tuning

$$Z_{IT} = \frac{Z_{LTC} Z_T}{Z_{LTC} + Z_T} \tag{4}$$

where  $Z_{LTC} = j\omega L_{TC}$  and  $Z_T$  is as given in Eq. (1).

### 2.3 Long Cable

In underwater acoustic systems, transducers are often connected to the power amplifier through long cables, which significantly affect the system's performance. The electrical resistance and the capacitance become significant for long cables [14]. The long cable is treated as a Transmission Line (TL) and is represented by the equivalent circuit shown in Fig. 5.

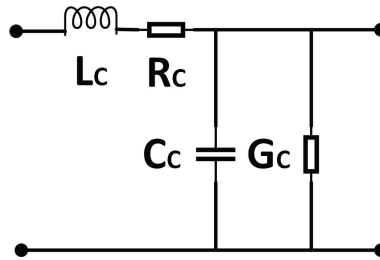


Fig. 5 Equivalent circuit of a cable

The cable parameters are determined by measuring the impedance spectra at one end of the cable by keeping the other end open and short conditions successively. The corresponding impedances are  $Z_1$  and  $Z_2$ , respectively. The characteristic impedance  $Z_C$  and the propagation constant  $\gamma_C$  of the cable are determined using the relations  $Z_C = \sqrt{Z_2/Z_1}$  and  $\gamma_C = \sqrt{Z_1 Z_2}$  [15, 16]. The cable parameters per meter, as shown in Fig. 5, are determined from the relations, where  $l$  is the length of the cable.

These values determined for 200 m long JDR make single core coaxial cable are given in Tab. 2. The characteristic impedance  $Z_C$  and phase velocity  $v_p$  of the cable are determined from, Eqs (5a-d)

$$R_C = \frac{\text{Re}(Z_C \gamma_C)}{l} \tag{5a}$$

$$L_C = \frac{\text{Im}(Z_C \gamma_C)}{\omega l} \tag{5b}$$

$$G_C = \frac{\text{Re}\left(\frac{Z_C}{\gamma_C}\right)}{l} \tag{5c}$$

$$C_C = \frac{\text{Im}\left(\frac{Z_C}{\gamma_C}\right)}{\omega l} \tag{5d}$$

$$Z_C = \sqrt{\frac{L_C}{C_C}} \quad (6)$$

$$v_p = \frac{1}{\sqrt{L_C C_C}} \quad (7)$$

and are found to be  $57 \Omega$  and  $1.78 \times 10^8$  m/s for the cable used in the present study.

*Tab. 2 Equivalent circuit parameter of the Cable*

Length $l$	Resistance $R_C$	Inductance $L_C$	Capacitance $C_C$	Conductance $G_C$
1 m	$0.107 \Omega$	$0.321 \mu\text{H}$	$98.7 \text{ pF}$	$12.8 \text{ nS}$

### 3 Design of Impedance Matching Network

The introduction of a long cable between the power amplifier and the tuned transducer eventually leads to impedance mismatch and power loss [17]. In addition to high power AC, high-speed data and high-voltage DC are also simultaneously transmitted through the same cable. The high power AC, high-speed data and high-voltage DC are coupled and decoupled to and from the single-core coaxial cable using a set of couplers and de-couplers shown in Fig. 1. The inclusion of reactive components, such as capacitors and inductors of the coupler and de-coupler circuits, introduces additional impedance mismatch in the network. Therefore, it is essential to compensate for the imbalances caused by (i) the long cable, (ii) the AC coupler, (iii) the DC coupler, and (iv) the data coupler by designing a suitable impedance-matching network [18, 19].

#### 3.1 Case I: Circuit with Cable, Tuning Coil, and Transducer

In this case, the power amplifier is connected to the tuned transducer through a long cable, which is shown in Fig. 6. The power amplifier is represented by a voltage source  $V_{in}$  in series with internal resistance  $R_{int}$ . The input impedance of the tuned transducer  $Z_{in}^I$  with the cable for *Case I* is written as

$$Z_{in}^I = R_C + Z_{L_C} + \frac{Z_{C_C} Z_{TT}}{Z_{C_C} + Z_{TT}} \quad (8)$$

where  $Z_{C_C} = \frac{1}{j\omega C_C}$  and  $Z_{L_C} = j\omega L_C$ .

#### 3.2 Case II: Circuit with Cable, ML, Tuning Coil, and Transducer

Here the impedance mismatch in the circuit caused by the long cable has been compensated for by the addition of a suitable matching line, as shown in Fig. 7. The impedance of the tuned transducer ( $Z_{TT}$ ), given in Eq. (4), is matched with the characteristic impedance of the cable ( $Z_C$ ) given by

$$Z_C = \frac{Z_{C_C} (R_C + Z_{L_C})}{Z_{C_C} + R_C + Z_{L_C}} \quad (9)$$

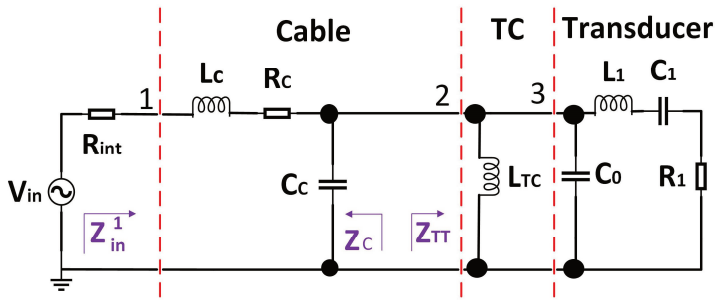


Fig. 6 Circuit with a long cable, tuning coil, and transducer (Case I)

$Z_c$  is calculated based on an assumption that  $R_{int}$  is much lower than  $R_c$ . In this paper  $R_{int}$  is taken as  $2.2 \Omega$ , which is the internal resistance of the power amplifier. The characteristic impedance of the matching line is determined by applying the principles of a quarter-wavelength transmission line [1]. Therefore,

$$Z_{ML}^{II} = \sqrt{Z_c + Z_{TT}} \tag{10}$$

The superscript ‘II’ refers to *Case II*. The quarter wavelength Matching Line (ML) length corresponding to the phase velocity of  $1.78 \times 10^8$  m/s and 5 kHz is about 9 km, which is impossible to implement in practice. Therefore, an equivalent matching line is synthesized using a T-network with approximately similar characteristics. The symmetric T-network is constituted by two inductors  $L_{ML}^{II}$  and a capacitor  $C_{ML}^{II}$ , as shown in Fig. 7. The values of inductor and capacitor per meter length for *Case II* are determined from

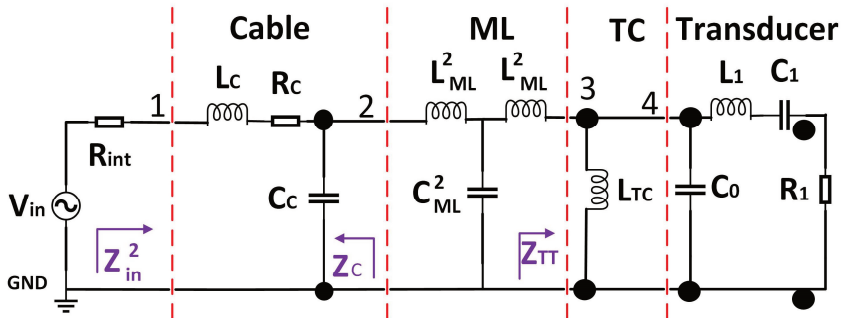


Fig. 7 Circuit with a long cable, matching line, tuning coil, and transducer (Case II)

$$L_{ML}^{II} = \frac{Z_{ML}^{II}}{v_p} \tag{11a}$$

$$C_{ML}^{II} = \frac{1}{Z_{ML}^{II} v_p} \tag{11b}$$

The net impedance of the circuit shown in Fig. 7 for *Case II* is determined by appropriately combining the impedances of all the individual branches. Therefore, input impedance  $Z_{in}^{II}$  of the circuit, as seen by the power amplifier for *Case II*, is

$$Z_{in}^{II} = \frac{Z_{C_C} \left[ \frac{Z_{C_{ML}}^{II} (Z_{L_{ML}}^{II} + Z_{T_T}^{II})}{Z_{C_{ML}}^{II} + Z_{L_{ML}}^{II} + Z_{T_T}^{II}} + Z_{L_{ML}}^{II} \right]}{Z_{C_C} + \frac{Z_{C_{ML}}^{II} (Z_{L_{ML}}^{II} + Z_{T_T}^{II})}{Z_{C_{ML}}^{II} + Z_{L_{ML}}^{II} + Z_{T_T}^{II}} + Z_{L_{ML}}^{II}} + R_C + Z_{L_C} \quad (12)$$

### 3.3 Case III: Circuit with Cable, AC Coupler, ML, Tuning Coil, and Transducer

An AC coupler is included with *Case II* circuit to couple high power AC signal through the long cable. The modified circuit is shown in Fig. 8 and the configuration is referred to as *Case III*. The AC coupler and de-coupler consist of two capacitors each on input and output sections of the long cable, respectively, as shown in Fig. 8. The introduction of coupling and decoupling capacitors in the circuit modifies the impedance and causes an imbalance in the impedance matching scheme. Therefore, the matching line (ML) is to be modified accordingly. The impedance of the long cable along with the AC coupler  $Z_C^{III}$  at the input section of the matching line, for *Case III*, at Node 2 in Fig. 8 is written as

$$Z_C^{III} = \frac{Z_{C_C} (R_C + Z_{C_{C_{1o}}} + Z_{C_{C_{2o}}} + Z_{L_C})}{R_C + Z_{C_C} + Z_{C_{C_{1o}}} + Z_{C_{C_{2o}}} + Z_{L_C}} + Z_{C_{C_{1r}}} + Z_{C_{C_{2r}}} \quad (13)$$

where  $Z_{C_{C_{ij}}} = \frac{1}{j\omega C_{C_{ij}}}$ ,  $i = 1$  to  $N$  and  $j = 'o'$  or  $'r'$ , we will use this parameter in the subsequent analysis. Where  $'o'$  is the onboard side and  $'r'$  is the remote side.

The characteristic impedance  $Z_C^{III}$  of the quarter wavelength matching line for *Case III* is determined from Eq. (14).

$$Z_{ML}^{III} = \sqrt{Z_C^{III} Z_{T_T}^{III}} \quad (14)$$

For *Case III*, values  $L_{ML}^{III}$  and  $C_{ML}^{III}$  in the matching line are determined by substituting  $Z_{ML}^{III}$  from Eq. (14) for  $Z_{ML}^{II}$  in Eqs 11(a) and 11(b). The input impedance  $Z_{in}^{III}$  of the circuit shown in Fig. 8 for *Case III*, as seen by the power amplifier, is determined by the Eq. (15).

$$Z_{in}^{III} = \frac{Z_{C_C} \left[ Z_{C_{C_{1r}}} + Z_{C_{C_{2r}}} + \frac{Z_{C_{ML}}^{III} (Z_{L_{ML}}^{III} + Z_{T_T}^{III})}{Z_{C_{ML}}^{III} + Z_{L_{ML}}^{III} + Z_{T_T}^{III}} + Z_{L_{ML}}^{III} \right]}{Z_{C_C} + Z_{C_{C_{1r}}} + Z_{C_{C_{2r}}} + \frac{Z_{C_{ML}}^{III} (Z_{L_{ML}}^{III} + Z_{T_T}^{III})}{Z_{C_{ML}}^{III} + Z_{L_{ML}}^{III} + Z_{T_T}^{III}} + Z_{L_{ML}}^{III}} + R_C + Z_{L_C} + Z_{C_{C_{1o}}} + Z_{C_{C_{2o}}} \quad (15)$$

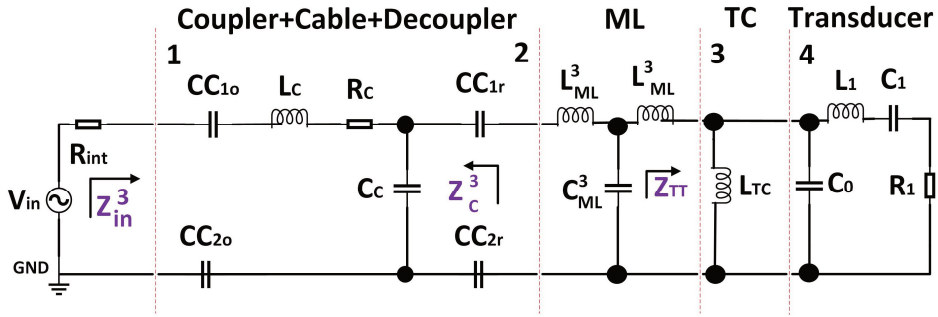


Fig. 8 The circuit with cable, AC coupler, matching line, tuning coil, and transducer (Case III)

### 3.4 Case IV: Circuit with Cable, AC Coupler DC Coupler Data Coupler, ML, Tuning Coil, and Transducer

In order to simultaneously transmit AC, DC, and data through the single core coaxial cable, AC coupler, DC coupler, and Data Coupler are added to the circuit of Case III. The modified circuit of Case IV is shown in Fig. 9. The couplers and de-couplers consist of a set of LC components connected in a specific configuration on either side of the long cable. The components on the onboard and remote sides are identified as ‘o’ and ‘r’ in their respective notations, as shown in Fig. 9.

Additional components in the circuit modify the impedance and offset the matching scheme. Therefore, the matching line has to be modified accordingly. The net impedance of the long cable along with the AC coupler, DC coupler, and Data Coupler  $Z_C^{IV}$  at the input section of the matching line at Node 2 in Fig. 9 is given in Eq. (16)

$$Z_C^{IV} = \frac{Z_e \left( R_C + \frac{Z_a Z_C C_{1o}}{Z_a + Z_C C_{1o}} + Z_b + Z_{LC} \right)}{R_C + Z_e + \frac{Z_a Z_C C_{1o}}{Z_a + Z_C C_{1o}} + Z_b + Z_{LC}} + Z_{C_{C1r}} + Z_{C_{C2r}} \quad (16)$$

where  $Z_e$ ,  $Z_a$ ,  $Z_b$ ,  $Z_c$  and  $Z_d$  are defined as

$$Z_a = \frac{(R_{1o} + Z_{L_{1o}})(R_{2o} + Z_{C_{3o}})}{R_{1o} + Z_{L_{1o}} + R_{2o} + Z_{C_{3o}}} \quad (17a)$$

$$Z_b = \frac{Z_{L_{2o}} Z_{C_{4o}} Z_{C_{C2o}}}{Z_{C_{C2o}} Z_{L_{2o}} + Z_{C_{C2o}} Z_{C_{4o}} + Z_{L_{2o}} Z_{C_{4o}}} \quad (17b)$$

$$Z_c = Z_{L_{1r}} + Z_{L_{2r}} + \frac{Z_{C_{1r}} R_{1r}}{Z_{C_{1r}} + R_{1r}} \quad (17c)$$

$$Z_d = Z_{C_{4r}} + Z_{C_{5r}} + \frac{Z_{L_{3r}} R_{2r}}{Z_{L_{3r}} + R_{2r}} \quad (17d)$$

$$Z_e = \frac{Z_{C_c} Z_c Z_d}{Z_{C_c} Z_c + Z_{C_c} Z_d + Z_c Z_d} \quad (17e)$$

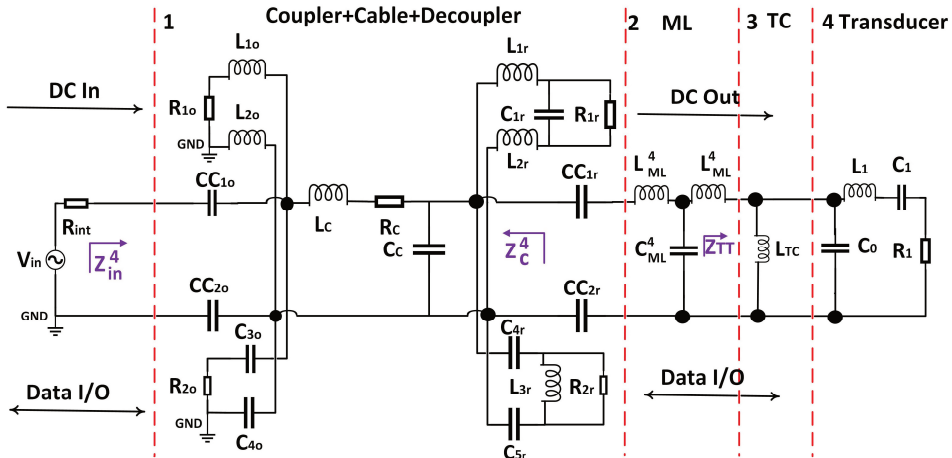


Fig. 9 Circuit with cable, AC coupler DC coupler and Data Coupler, matching line, tuning coil, and transducer (Case IV)

The characteristic impedance of the matching line, in this case, is determined from

$$Z_{ML}^{IV} = \sqrt{Z_C^{IV} + Z_{TT}} \quad (18)$$

The  $L_{ML}^{IV}$  and  $C_{ML}^{IV}$  in the matching line for Case 4 are determined by substituting  $Z_{ML}^{IV}$  from Eq. (18) for  $Z_{ML}^1$  in Eq. (11). The input impedance  $Z_{in}^{IV}$  of the circuit shown in Fig. 9 for Case IV, as seen by the power amplifier, is given by the Eq. (19).

The values of inductances and capacitances of the quarter wavelength matching lines corresponding to the three cases are determined using the procedure described in this section and are given in Tab. 3. The numbers in the brackets are the nearest available values used in subsequent experimental validation.

Tab. 3 Calculated values of the matching line components for three cases. The nearest practically used values are given in brackets

Parameters	Case II	Case III	Case IV
$L_{ML}$ [mH]	6.2 (6.20)	6.8 (6.9)	6.8 (6.9)
$C_{ML}$ [ $\mu$ F]	0.177 (0.18)	0.201 (0.2)	0.201 (0.2)

$$Z_{in}^{IV} = \frac{Z_a \left\{ R_C + Z_b + \frac{Z_e \left[ Z_{CC1r} + Z_{CC2r} + \frac{Z_{CML}^{IV} (Z_{LML}^{IV} + Z_{TT}^{IV})}{Z_{CML}^{IV} + Z_{LML}^{IV} + Z_{TT}^{IV}} + Z_{LML}^{IV} \right]}{Z_{CC1r} + Z_{CC2r} + \frac{Z_{CML}^{IV} (Z_{LML}^{IV} + Z_{TT}^{IV})}{Z_{CML}^{IV} + Z_{LML}^{IV} + Z_{TT}^{IV}} + Z_{LML}^{IV} + Z_e} \right\} + Z_{LC}}{Z_a + R_C + Z_b + \frac{Z_e \left[ Z_{CC1r} + Z_{CC2r} + \frac{Z_{CML}^{IV} (Z_{LML}^{IV} + Z_{TT}^{IV})}{Z_{CML}^{IV} + Z_{LML}^{IV} + Z_{TT}^{IV}} + Z_{LML}^{IV} \right]}{Z_{CC1r} + Z_{CC2r} + \frac{Z_{CML}^{IV} (Z_{LML}^{IV} + Z_{TT}^{IV})}{Z_{CML}^{IV} + Z_{LML}^{IV} + Z_{TT}^{IV}} + Z_{LML}^{IV} + Z_e} + Z_{LC}} + Z_{CC1o} \quad (19)$$

## 4 Power Calculation

The theoretical analysis of the electrical power drawn by the circuits for a given transducer from the power amplifier for four different cases is presented in this section. These results have been verified by MultiSim simulation studies and validated by experiments.

### 4.1 Theoretical Analysis

The input impedances of the circuits are shown in Figs 6-9. A power amplifier drives the high power AC signals into the circuit at their respective Node 1. The power amplifier supplies an RMS voltage of  $V_{in}$  to the load with input impedance  $Z_{in}$ . Therefore, the input electrical power drawn by the respective circuits is given by

$$P_{in}^i = \frac{V_{in}^2}{Z_{in}^i} \quad (20)$$

where  $i = I, II, III, IV$  for the four cases studied.

### 4.2 MultiSim Simulation Studies

Theoretical analysis using an equivalent circuit model has been verified by simulation studies carried out using a simulation software tool Multisim 14.2. The circuits shown in Figs 6-9 are analyzed with the circuit parameter values given in Tab. 4.

### 4.3 Experimental Validation

Experiments further validate the modeled results. The prototype circuits with various combinations shown in Figs 6-9 have been made, and their characteristics are measured using the experimental setup shown in Fig. 10(a). Photographs of the transducer, tuning coil, matching lines, 200 m long cable, the couplers, the data acquisition system, and power amplifier are shown in Fig. 10(b).

The experimental setup consists of an acoustic tank in which the test transducer and a standard hydrophone are positioned at 6 m deep in water with a separation of 8 m. The transducer is connected to the power amplifier (Make: Instruments Inc, Model: L10) through the tuning coil, matching line, 200 m long cable, and the respective couplers at the remote unit.

Tab. 4 Values of various components of the circuits shown in Figs 7-9

Parameter	Unit	Case II	Case III	Case IV
$C_{C_{1o}}, C_{C_{2o}}$	$\mu\text{F}$	–	3.3	3.3
$R_{\text{int}}$	$\Omega$	10	10	10
$C_{3o}$	nF	–	–	10
$C_{4o}$	nF	–	–	10
$R_{2o}$	$\Omega$	–	–	20
$L_{1o}, L_{2o}$	mH	–	–	600
$R_{1o}$	$\Omega$	–	–	44
$L_{1r}, L_{2r}$	mH	–	–	600
$C_{1r}$	$\mu\text{F}$	–	–	100
$R_{1r}$	$\Omega$	–	–	200
$C_{C_{1r}}, C_{C_{2r}}$	$\mu\text{F}$	–	3.3	3.3
$L_{\text{ML}}$	mH	6.2	6.9	6.9
$C_{\text{ML}}$	$\mu\text{F}$	0.2	0.3	0.2
$L_{\text{TC}}$	mH	20.6	20.6	20.6
$C_{4r}, C_{5r}$	nF	–	–	10
$L_{3r}$	mH	–	–	1
$R_{2r}$	$\Omega$	–	–	50

The signal for high power transmission is generated by the data acquisition and processing system and it is fed to the power amplifier. From the power amplifier, the high power AC signals are coupled to the cable through an AC coupler. The high power signal is decoupled from the high voltage DC and high-speed data transmitted through the cable. At the remote end, the transducer further generates the high power acoustic signals. These acoustic signals are received by a standard hydrophone and fed to the data acquisition and processing unit (NI and LabVIEW) through a preamplifier (B&K Nexus). The input electrical impedance spectra are determined from the voltage and current information of the transmitted signals. The acoustic characteristics, namely, Transmitting Voltage Response (TVR) and Source Level (SL) of the transducer with all associated circuits, are measured using the setup shown in Fig. 10. *Case I* is a cable with Tuning coil ( $L_{\text{TC}}$ ) and sensor, *case II* is a cable with Tuning coil, matching line and sensor, *case III* is a cable with AC Coupler, tuning coil, ML and sensor, *case IV* is a cable with AC coupler DC coupler Data Coupler, tuning coil, ML and sensor. The voltage at the power amplifier's output is maintained constant at 125 V throughout the frequency band of interest. Input power is determined from the power amplifier's output voltage and current that drive the circuits under different configurations described in section 3.

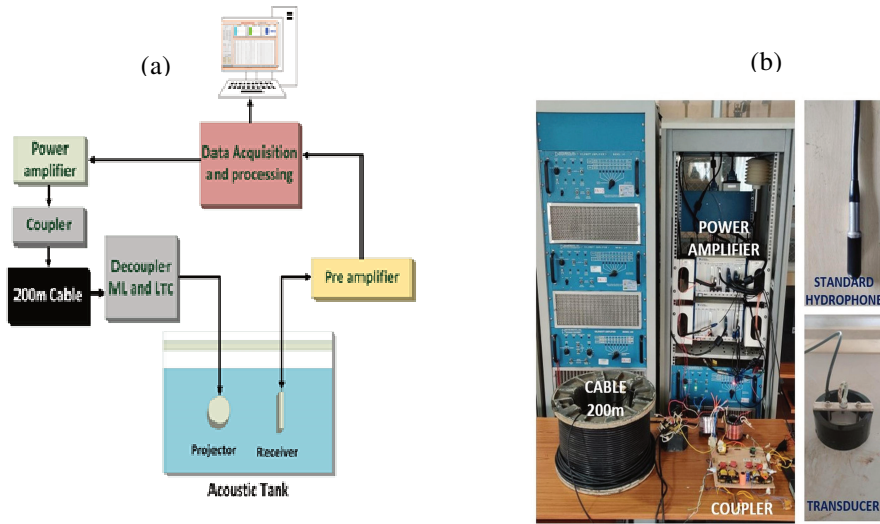


Fig. 10 (a) Schematic diagram of the experimental setup for measuring the characteristics of the circuits with various combinations (b) Photograph showing power amplifier, couplers, cable, matching line, tuning coil, and transducer. The transducer is deployed at 6 m deep in the tank during evaluation

## 5 Results and Discussions

### 5.1 Impedance and Power

The input impedance, electrical power, and power factor of the circuits calculated using the theoretical model, MultiSim simulation studies, and experiments are shown in Figs 6-9 while Fig. 11 shows their comparisons. The input impedances  $Z_{in}^I$ ,  $Z_{in}^{II}$ ,  $Z_{in}^{III}$ , and  $Z_{in}^{IV}$  of the circuits shown in Figs 6-9, respectively, are determined at Node 1 using Eqs (9), (13), (16), and (20). The corresponding impedance spectra are shown in Fig. 11(a) and they are compared with the results of MultiSim simulation and experimental studies. The impedance magnitudes are found to be about  $40 \Omega$  at the resonance frequency of 4 770 Hz. The impedance magnitude for MultiSim simulation and measurement is found to be about  $40 \Omega$  and  $50 \Omega$  at the resonance of 4 745 Hz and 4 800 Hz, respectively.

Variations in the input power determined from Eq. (20) for the four cases are shown in Fig. 11(b). For *Case II*, it is clear from Fig. 11(b) that the maximum power reaches about 240 W and 234 W for theoretical and MultiSim simulation studies, respectively, and the measured power is 286 W. The estimated power spectra show broadband response, whereas the measured spectrum shows a single peak at resonance. For the circuit with an AC coupler (*Case III*), the theoretical and MultiSim simulation plots show that the maximum power is approximately 248 W, and the measured power is 303.69 W. For the circuit with AC coupler, DC coupler, and Data Coupler (*Case IV*), the power calculated from the theoretical and simulated analysis is 247 W, and the experimental value is about 320 W. The resonance frequency in the experimental plot shows a shift from 4 760 Hz to 4 600 Hz. This is due to the differ-

ence in the actual component values of ML, and the tuning coil taken for experimental studies from the required ones, as given in Tab. 3.

The Power Factor (PF), which is the ratio of actual power to the apparent power, is also calculated from Eq. (2) and shown in Fig. 11(c) along with the MultiSim simulation and experimental results for various cases. The bare transducer is capacitive and lossy with a very low value of PF, which is improved by connecting a suitably designed tuning coil. Adding a long cable decreases the PF, which is again improved by adding suitable matching lines. It is to be noted that the introduction of matching lines increases the PF close to unity over a wideband band of frequencies for all three cases except *case 1*. This is advantageous and would result in significant improvements in the system performance.

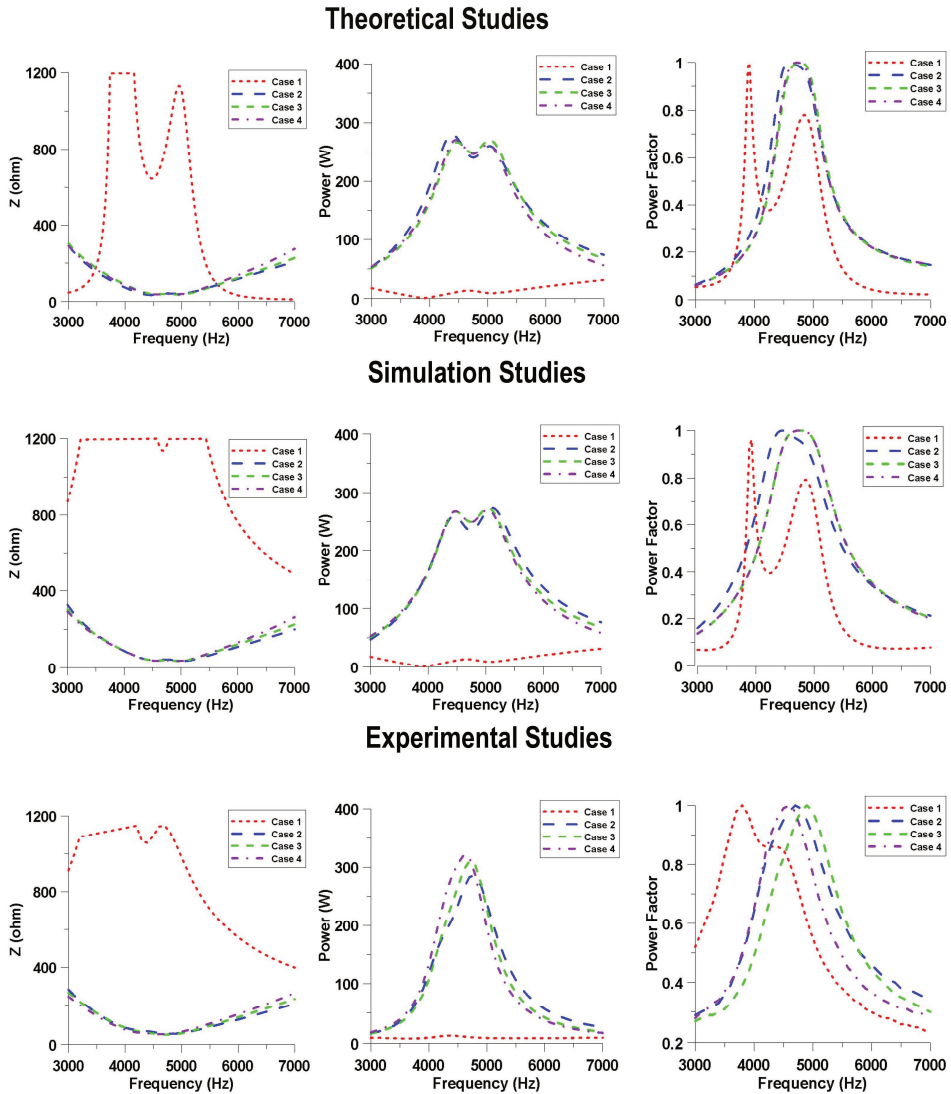


Fig. 11 (a) Input impedance spectra (b) power and (c) power factor for four cases

### 5.2 Sensitivity Analysis

The effect of deviations in the inductor values of the T-network constituting the matching lines has been studied by intentionally varying the  $L_{ML}^{IV}$  values and determining the input power. Sensitivity analysis has been carried out with  $L_{ML}^{IV}$  values of 6.2 mH, 6.9 mH, and 8 mH. Fig. 12 shows the corresponding power spectra. It is observed that any error in the  $L_{ML}^{IV}$  value strongly affects the power. The peak power and the corresponding resonance frequency decrease by about 80 W and 500 Hz, respectively, as  $L_{ML}^{IV}$  is increased from 6.2 mH to 8 mH. Therefore, the component values of the matching lines should be exactly the same as the design values for accurate results.

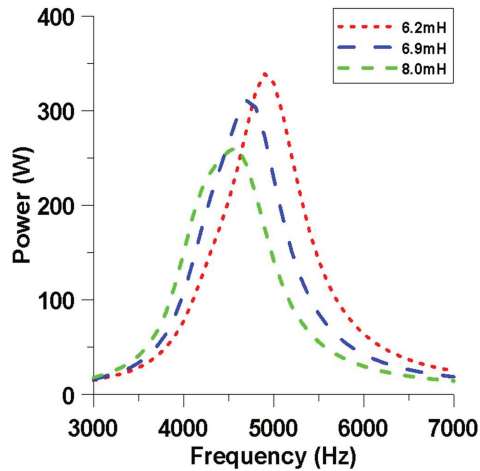


Fig. 12 Effect of deviations in inductance value of the matching line

### 5.3 Acoustic Response

It is important that the addition of long cables, couplers and decouplers to the circuit for the implementation of the proposed telemetry scheme does not affect the acoustic characteristics of the overall systems. Hence, the influence of additional components and compensating mechanisms presented has been studied.

The main characteristics of an acoustic system are the Transmitting Voltage Response (TVR) [5, 20-22], and the Source Level (SL) [21, 22]. TVR is the ratio of the acoustic pressure which the transducer generates in water in response to 1 V input, and SL is the maximum pressure which the transducer can generate before reaching the non-linear stage. TVR and SL of the transducer with various configurations shown in Figs 6-9 are measured using the setup shown in Fig. 10(a) using the comparison calibration method [21]. The results of SL and TVR are shown in Fig. 13(a) and Fig. 13(b). With *case I*, the SL and TVR is low and it comes around ~177 dB and ~133 dB at resonance. With the introduction of ML (*case II*), the SL and TVR increase by more than 10 dB for a constant input voltage of 125 Vrms from power amplifier. By the inclusion of coupler and decoupler to the circuit at onboard and remote side, the SL and TVR decrease by 2 dB, which is unavoidable.

A lumped-parameter electrical equivalent circuit model has been developed to analyze the underwater acoustic transmitting system that consists of a power amplifier, a long cable, and an underwater acoustic transducer. In order to minimize the power loss through the long cable with AC coupler, DC coupler, and Data Coupler, an impedance matching scheme is proposed. The theoretical model has been verified by MultiSim simulation studies and validated by experiments. The impedance matching network scheme proposed in the present work is also found to significantly enhance the power by 300 W, power factor to 100 %, and TVR and SL by about 10 dB at resonance for a constant input voltage of 125 V.

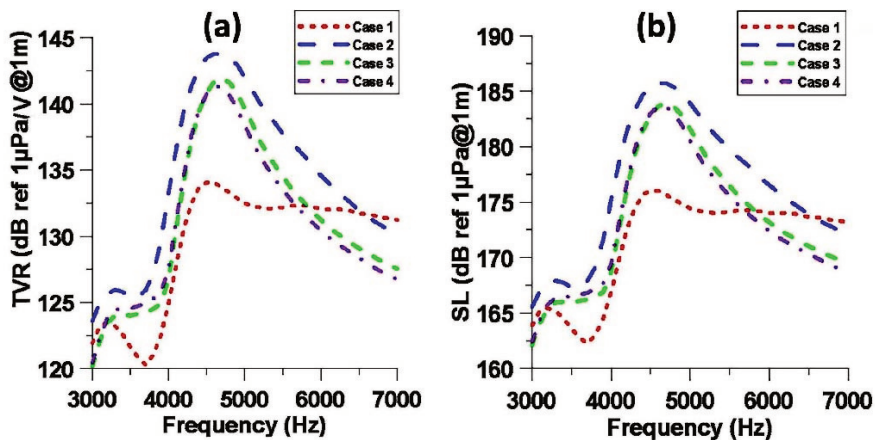


Fig. 13 Comparison of measured (a) Transmitting voltage response (TVR) (b) Source Level (SL) for four cases.

## 6 Conclusion

A lumped-parameter electrical equivalent circuit model is developed to analyze the underwater acoustic transmitting system that consists of a power amplifier, a long cable, and an underwater acoustic transducer. In order to minimize the power loss through the long cable with AC-DC Data couplers, an impedance matching scheme is proposed. The theoretical model is verified by network simulation studies and validated by experiments. The impedance matching network scheme proposed in the present work is found to significantly enhances the power by 300 W, power factor to 100 %, and TVR and SL by about 10 dB at resonance for a constant input voltage of 125 V.

## Acknowledgement

The authors thank the Director, NPOL, Kochi, for providing facilities and permission to publish this work. They also thank Unikkat Ganeshan, Harry P.R, O.B. Sathesh and R. Krishnakumar for help in acoustic measurements.

## References

- [1] RATHOD, V.T. A Review of Electric Impedance Matching Techniques for Piezoelectric Sensors, Actuators and Transducers. *Electronics*, 2019, **8**(2), 169. DOI 10.3390/electronics8020169.
- [2] JIAN, X., Z. LI, Z. HAN, J. XU, P. LIU, Y. LIU, Y. CUI and W. HUANG. The Study of Cable Effect on High-Frequency Ultrasound Transducer Performance. *IEEE Sensors Journal*, 2018, **18**(13), pp. 5265-5271. DOI 10.1109/JSEN.2018.2838142.
- [3] HUANG, H and D. PARAMO. Broadband Electrical Impedance Matching for Piezoelectric Ultrasound Transducers. *IEEE Transactions Ultrasonics Ferroelectric Frequency Control*, 2011, **58**(12), pp. 2699-2707. DOI 10.1109/TUFFC.2011.2132.
- [4] MANOJ, G., E. JACOB and S. KUNDUKULAM. Relay based Coupling Scheme of High Speed Communication Data, High Voltage DC and High Power Pulsed AC for Coaxial Cable. *Defence Science Journal*, 2018, **68**(5), pp. 487-493. DOI 10.14429/dsj.68.11907.
- [5] RADKE, H.N. Development of a Self-Tuning Amplifier for Piezoelectric Transducer Evaluations [online]. *Open Access Master's Theses*, 2013, Paper 80. [viewed 2021-11-09]. Available from: <https://digitalcommons.uri.edu/cgi/viewcontent.cgi?article=1077&context=theses>
- [6] RAMESH, R. and D.D. EBENEZER. Equivalent Circuit for Broadband Underwater Transducers. *IEEE Transactions Ultrasonics Ferroelectric Frequency Control*, 2008, **55**(9), pp. 2079-2083. DOI 10.1109/TUFFC.899.
- [7] XIYOU, C., L. GUANLIN, M. XIANMIN and X. KANG. The Design of Impedance Matching between Long Cable and Ultrasonic Transducer under Seawater. In: *IECON 2016 - 42<sup>nd</sup> Annual Conference of the IEEE Industrial Electronics Society*. Florence: IEEE, 2016, pp. 4576-4581. DOI 10.1109/iecon.2016.7793135.
- [8] DECARPIGNY, J.N., B. HAMONIC and O.B. WILSON. The Design of Low Frequency Underwater Acoustic Projectors: Present Status and Future Trends. *IEEE Journal of Ocean Engineering*, 1991, **16**(1), pp. 107-122. DOI 10.1109/48.64890.
- [9] GRACIA-RODRIGUEZ, M., J. GARCÍA-ÁLVAREZ, Y. YANEZ, GM.J. ARCA-HERNANDEZ, J. SALAZAR, A. TURO and J.A. CHÁVEZ. Low Cost Matching Network for Ultrasonic Transducers. *Physics Procedia*, 2010, **3**(1), pp. 1025-1031. DOI 10.1016/j.phpro.2010.01.132.
- [10] EBENEZER, D.D. and N. RAVI. An Equivalent Circuit Approach to Determine the In-Situ Radiation Impedance of Underwater Electroacoustic Projectors. *Journal of the Acoustical Society of India*, 1993, **21**(2), pp. 110-115. ISSN 0973-3302.
- [11] KUMAR, M.A., R.M. ABRAHAM, R. RAMESH, K.P.B. MOOSAD and D.D. EBENEZER. Design and Development of Flexural Disc Projector for Low Frequency Sonar Applications. In: *2013 Ocean Electronics (SYMPOL)*. Kochi: IEEE, 2013. DOI 10.1109/sympol.2013.6701946.
- [12] JIN, H., S.R. DONG, J.K. LUO and W.I. MILNE. Generalised Butterworth-Van Dyke Equivalent Circuit for Thin-Film Bulk Acoustic Resonator. *Electronics Letter*, 2011, **47**(7), pp. 424-426. DOI 10.1049/el.2011.0343.

- 
- [13] RAMESH, R., S.S. PILLAI, P. ABRAHAM and D.D. EBENEZER. Characteristics of Broadband Underwater Transducers Integrated with Tuning Coils and Cables. In: *2009 International Symposium on Ocean Electronics (SYMPOL 2009)*. Kochi: IEEE, 2009, pp. 133-138. DOI 10.1109/sympol.2009.5664172.
- [14] SAFARI, A. and E.K. AKDOGAN. *Piezoelectric and Acoustic Materials for Transducer Applications*. New York: Springer, 2008. ISBN 978-0-387-76538-7.
- [15] SHI, Q., U. TRÖLTZSCHAND and O. KANOUN. Analysis of the Parameters of a Lossy Coaxial Cable for Cable Fault Location. In: *Eighth International Multi-Conference on Systems, Signals & Devices*. Sousse: IEEE, 2011. DOI 10.1109/SSD.2011.5767393.
- [16] FANG, W., Y. REN, X. LIU, X. JIAO and C. CHU. Parameter Extraction Method for the Twisted Pair Cable With Rectangular Connectors. *PLoS One*, 2018, **13**(10), e0205072. DOI 10.1371/journal.pone.0205072.
- [17] ZHOU, H., S.H. HUANG and W. LI. Electrical Impedance Matching Between Piezoelectric Transducer and Power Amplifier. *IEEE Sensors Journal*, 2020, **20**(23), pp. 14273-14281. DOI 10.1109/JSEN.2020.3008762.
- [18] GOMEZ, F.R. Design of Impedance Matching Networks for RF Applications. *Asian Journal of Engineering and Technology*, 2018, **6**(4). DOI 10.24203/ajet.v6i4.5450.
- [19] WANG, B., Z. CAO and F. SONG. Design and Evaluation of a T-Shaped Adaptive Impedance Matching System for Vehicular Power Line Communication. *IEEE Access*, 2020, **8**, pp. 73843-73854. DOI 10.1109/ACCESS.2020.2988299.
- [20] DENG, Y., G. ZHANG and X. ZHANG. A Method to Depress the Transmitting Voltage Response Fluctuation of a Double Excitation Piezoelectric Transducer. *Applied Acoustics*, 2020, **158**, 107066. DOI 10.1016/j.apacoust.2019.107066.
- [21] SHERMAN, C.H. and J.L. BUTLER. *Transducers and Arrays for Underwater Sound*. New York: Springer, 2007. ISBN 978-1-4419-2198-7.
- [22] BOBBER, R.J. *Underwater Electroacoustic Measurements*. Baileys Harbor: Peninsula Pub, 1990. ISBN 978-0-932146-19-8.